ACSNANO
www.acsnano.org
ARTICLE

ZnO Quantum Dot Decorated Zn_2SnO_4 Nanowire Heterojunction Photodetectors with Drastic Performance Enhancement and Flexible Ultraviolet Image Sensors

Ludong Li,[†,‡,§] Leilei Gu,[¶,§] Zheng Lou,[†] Zhiyong Fan,[*,¶] and Guozhen Shen[*,†,‡]

[†]State Key Laboratory for Superlattices and Microstructures, Institute of Semiconductors, Chinese Academy of Sciences, Beijing 100083, China

[‡]College of Materials Science and Optoelectronic Technology, University of Chinese Academy of Sciences, Beijing 100029, China

[¶]Department of Electronic and Computer Engineering, The Hong Kong University of Science and Technology, Clear Water Bay, Kowloon, Hong Kong SAR, China

Supporting Information

ABSTRACT: Here we report the fabrication of high-performance ultraviolet photodetectors based on a heterojunction device structure in which ZnO quantum dots were used to decorate Zn_2SnO_4 nanowires. Systematic investigations have shown their ultrahigh light-to-dark current ratio (up to 6.8×10^4), specific detectivity (up to 9.0×10^{17} Jones), photoconductive gain (up to 1.1×10^7), fast response, and excellent stability. Compared with a pristine Zn_2SnO_4 nanowire, a quantum dot decorated nanowire demonstrated about 10 times higher photocurrent and responsivity. Device physics modeling showed that their high performance originates from the rational energy band engineering, which allows efficient separation of electron−hole pairs at the interfaces between ZnO quantum dots and a Zn_2SnO_4 nanowire. As a result of band engineering, holes migrate to ZnO quantum dots, which increases electron concentration and lifetime in the nanowire conduction channel, leading to significantly improved photoresponse. The enhancement mechanism found in this work can also be used to guide the design of high-performance photodetectors based on other nanomaterials. Furthermore, flexible ultraviolet photodetectors were fabricated and integrated into a 10 × 10 device array, which constitutes a high-performance flexible ultraviolet image sensor. These intriguing results suggest that the band alignment engineering on nanowires can be rationally achieved using compound semiconductor quantum dots. This can lead to largely improved device performance. Particularly for ZnO quantum dot decorated Zn_2SnO_4 nanowires, these decorated nanowires may find broad applications in future flexible and wearable electronics.

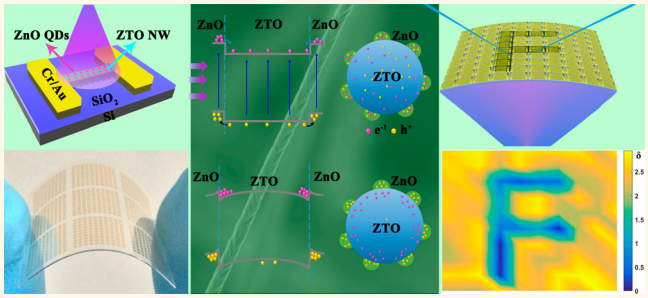

KEYWORDS: *Zn_2SnO_4 nanowires, ZnO quantum dots, photodetectors, flexible electronics, image sensors*

Over the past decades, ultraviolet (UV) sensing technology has triggered enormous interest because of its wide applications in crime investigation, oil spill detecting, fire monitoring, and electrical power line inspection.[1−5] Moreover, flexible UV image sensors can be applied in much wider range applications because of their attractive features of being flexible, portable, and wearable.[6−9] However, due to the low signal intensity of UV radiation in many practical applications, high-performance flexible UV photodetectors are critical to realize flexible UV imaging.[10] So far, various wide-band-gap semiconductor materials have been explored to fabricate UV photodetectors, such as III-nitrides,[11−13] II−VI compounds,[14−16] III−VI compounds,[17,18] and IV−VI compounds.[19,20] Among these wide-band-gap semiconductor materials, metal oxides have been extensively investigated because of their abundant reserves, excellent stability, and environmentally benign nature.[21] Furthermore, metal oxide semiconductors with one-dimensional (1-D) nanostructures show much higher photoresponse compared with their bulk or thin-film counterparts due to the large specific surface area, high aspect ratio, and small feature size

Received: February 2, 2017
Accepted: March 21, 2017
Published: March 21, 2017

DOI: 10.1021/acsnano.7b00749
ACS Nano 2017, 11, 4067−4076

comparable to the Debye screening length.[21−25] Up to now, many exciting results have been reported for the UV photodetectors based on 1-D binary metal oxide nanostructures.[15−20] For example, Yang *et al.* reported individual ZnO nanowire (NW) UV photodetectors, which displayed the potential application of ZnO NWs as optoelectronic switches.[15] Zhou *et al.* constructed single In_2O_3 NW UV photodetectors, which showed a substantial increase in conductance of up to 4 orders of magnitude.[18] Fang *et al.* fabricated individual thin SnO_2 NW UV photodetectors, which exhibited excellent light selectivity and ultrahigh external quantum efficiency (EQE).[20] However, most of the photodetectors based on pristine 1D binary metal oxide nanostructures have slow response (∼seconds), which greatly limits their practical applications, particularly for ZnO.[10,21,22,26]

As one of the most widely studied ternary metal oxides, Zn_2SnO_4 (ZTO) is an important n-type semiconductor material with a wide direct band gap of ∼3.64 eV.[26−28] It is also an earth-abundant material, which makes it suitable for the fabrication of low-cost electronic devices.[27] Due to their high electron mobility, fascinating optical properties, and high response speed, ZTO NWs display great application potency in UV photodetectors.[28] Nevertheless, the photoconductive gain of ZTO NWs is relatively low, which limits their practical application as UV photodetectors.[26,28]

Compared with single-component materials, 1-D materials with heterostructures usually can not only demonstrate the characteristics inherited from each component but also exhibit some additional attractive properties due to the interplay occurring at the interface of each component.[14,29] To improve the photoconductive gain of ZTO NWs, fabricating heterostructured NWs with high photoconductive gain materials can be a potential choice. As a high-photoconductive gain material, ZnO, with wide direct band gap of ∼3.26 eV, has a small lattice mismatch with ZTO, and it can be grown into various nanostructures easily and thus is suitable for such heterostructures.[10,26] However, considering the low response speed and high electrical conductivity of ZnO, ZnO-sheathed ZTO core/shell heterostructured NWs may not be the ideal structure for UV detection, as it will increase the response time and the dark current of ZTO NWs.

Here, ZnO quantum dot (QD) decorated ZTO NWs were synthesized *via* a facile two-step method. Systematic investigations on the photoresponse characteristics of individual ZnO QD decorated ZTO NW photodetectors based on a rigid SiO_2/Si substrate have shown their ultrahigh light−dark current ratio, specific detectivity and photoconductive gain, high response speed, excellent thermal stability, and long-term stability. Compared with a pristine ZTO NW, a QD-decorated NW demonstrated about 10 times higher photocurrent and responsivity. Device physics modeling showed that their appealing performance originates from the rational energy band engineering at the interfaces between ZnO QDs and ZTO NW, which allows efficient separation of electron−hole pairs at the interfaces. As a result of band engineering, holes migrate to QDs, which increases electron concentration and lifetime in the NW conduction channel, leading to a significantly improved photoresponse. At the same time, the trapped holes in ZnO QDs can increase the potential of the QDs, thus leading to a positive local gating effect, which further increases NW channel electron concentration. In addition, the flexible UV photodetectors were fabricated and integrated into a 10 × 10 array, which demonstrated the application as a high-performance flexible UV image sensor. The results indicate that the ZnO QD/ZTO NW heterostructure has a promising application potential in future flexible UV imaging technology. This device structure can also inspire fabrication of other types of NW-based high-performance photodetectors targeting at different wavelengths.

RESULTS AND DISCUSSION

The single-crystalline ZTO NWs were synthesized *via* a chemical vapor deposition method, which follows a vapor−liquid−solid (VLS) growth mechanism. The detailed synthesis process was described in the Methods section. Figure 1a,b show

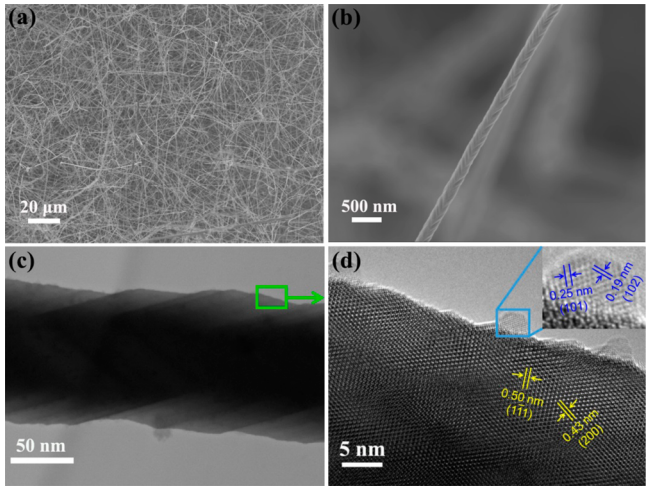

Figure 1. Materials characterization. (a, b) SEM images of ZTO NWs; (c) TEM image; (d) HRTEM image of ZTO NW with ZnO QDs. The inset is an enlarged view of the blue rectangle area in (d).

different magnification scanning electron microscopy (SEM) images of the as-prepared NWs. It can be seen that a large quantity of freestanding NWs was successfully synthesized on the substrate and the typical diameter and length of the NWs are about 100−300 nm and tens of micrometers, respectively. Moreover, periodical texture along the axial direction can be seen on the surface of NWs (Figure 1b), which appears like a bundle of inlaid rhombohedral nanocrystals along the axial direction of the NWs. This surface morphology in fact is similar to the ZTO NWs in previous reports.[28,30] The energy-dispersive X-ray (EDX) spectrum of a NW was shown in Figure S1a, which reveals that the NW is composed of Zn, Sn, and O elements, considering that the signals of C and Cu elements are from the transmission electron microscopy (TEM) grid. The X-ray diffraction (XRD) pattern (Figure S1b) further confirms that the as-synthesized NWs are face-centered cubic (FCC) spinel ZTO (JCPDS Card No. 24-1470). In addition, the XRD pattern shows that there are small quantities of SnO_2 in the as-synthesized sample. However, it appears that the ZTO NWs are of excellent crystallinity here since the SnO_2 peaks are of low frequency and intensity.

Through a facile solvothermal method,[31] the ZnO QDs were decorated onto ZTO NWs. Figure 1c depicts the TEM image of a single ZTO NW with ZnO QDs. From the high-resolution TEM (HRTEM) images in Figure S2b,c, it can be clearly seen that there are many hemispheric QDs on the surface of the ZTO NW, and the diameter of most QDs is less than 10 nm. The scanning TEM (STEM) image and the corresponding EDX elemental mapping are displayed in Figure S2d−g. It can

DOI: 10.1021/acsnano.7b00749
ACS Nano 2017, 11, 4067−4076

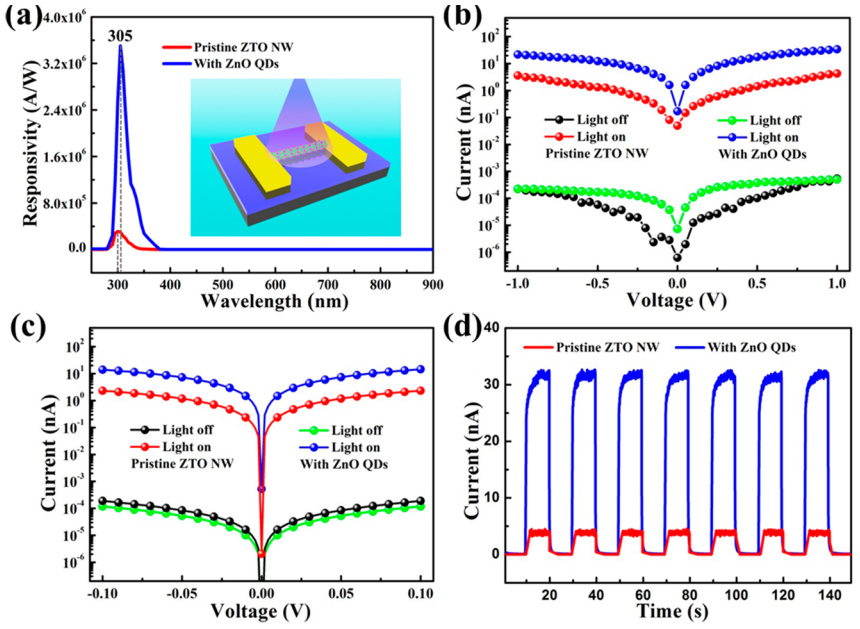

Figure 2. Performance characterization of the photodetectors. (a) Spectral responsivity of photodetectors made of a pristine ZTO NW and a ZnO QD decorated ZTO NW at different wavelengths ranging from 250 to 900 nm at a bias voltage of 1 V. The inset is the schematic illustration of the as-fabricated photodetector on a SiO_2/Si substrate. (b) $I-V$ curves of two kinds of photodetectors under dark and 300 nm UV illumination with a light intensity of 0.67 μW/cm^2. (c) Simulated $I-V$ curves of two kinds of photodetectors under dark and 300 nm UV illumination with a light intensity of 0.67 μW/cm^2. (d) Time-domain photoresponse of two kinds of photodetectors at a bias voltage of 1 V with a light intensity of 0.67 μW/cm^2.

be observed that the NW is composed of Zn, Sn, and O elements; however, the QD only shows a trace of Zn and O elements, which confirms the QD is ZnO. Figure 1d displays the HRTEM image zoomed in from the green rectangle area shown in Figure 1c, which shows the single-crystalline nature of the as-synthesized ZTO NW. The lattice constants observed from the ZTO NW were 0.50 and 0.43 nm, in agreement with the $(1\bar{1}1)$ and (200) planes of the spinel ZTO phase, respectively. The magnified lattice view of the ZnO QD is shown in the inset of Figure 1d, and the lattice spacing values of 0.25 and 0.19 nm are assigned to the (101) and (102) planes of the hexagonal wurtzite ZnO phase (JCPDS Card No. 36-1451).

In order to study the photoresponse characteristics of the ZnO QD decorated ZTO NWs, the photodetectors based on an individual pristine ZTO NW and individual ZnO QD decorated ZTO NW were fabricated by a conventional photolithographic process, as described in the Methods section. The schematic illustration of a ZnO QD decorated ZTO NW photodetector on a SiO_2/Si substrate is shown in the inset of Figure 2a. It can be seen that two electrodes (Cr/Au, 10/50 nm) were deposited on each end of the NW, the gap between them was about 10 μm, and the uncovered part of the NW was illuminated optically. Figure 2a depicts the spectral responsivity of photodetectors made of the pristine ZTO NW and the ZnO QD decorated ZTO NW at different wavelengths ranging from 250 to 900 nm at a bias voltage of 1 V. As an important figure-of-merit of photodetectors, the spectral responsivity can be defined as $R_\lambda = \Delta I/PS = (I_{light} - I_{dark})/PS$, where I_{light} is the light current, I_{dark} is the dark current, P is the incident light intensity, and S is the effective irradiated area.[14] As shown in Figure 2a, the spectral response of the two kinds of photodetectors was observed only in the ultraviolet region, with almost zero response observed in the visible and near-infrared region, which indicates their excellent wavelength selectivity. Moreover, it can be clearly seen that the spectral responsivity of the ZnO QD decorated ZTO NW photodetector is 11 times higher than the pristine ZTO NW photodetector at 305 nm and 8 times higher at 300 nm. This confirms that decorating ZnO QDs on ZTO NWs can significantly enhance their photoresponse in the ultraviolet region. In addition, the spectral response range of the pristine ZTO NW photodetector is approximately from 280 to 345 nm, and the peak value is at 300 nm. However, the spectral response range of the ZnO QD decorated ZTO NW photodetector is approximately from 280 to 380 nm, and the peak value is at 305 nm. This phenomenon is caused by the fact that the band gap of ZnO (3.26 eV) is smaller than the band gap of ZTO (3.64 eV); thus the spectral response range of the ZnO QD decorated ZTO NW photodetector is enlarged marginally, and the peak value shows a slight red shift. Figure 2b displays the comparative $I-V$ curves of two kinds of photodetectors under dark and 300 nm UV illumination with a light intensity of 0.67 μW/cm^2. The light current of the device with ZnO QDs is almost 1 order of magnitude higher than the other one, whereas the dark current levels of two devices are close. Besides spectral responsivity (R_λ), light-to-dark current ratio (I_{light}/I_{dark}), specific detectivity (D^*), and photoconductive gain (G) are also key figures-of-merit defining the performance of photodetectors. The definitions of specific detectivity (D^*) and photoconductive gain (G) can be found in the previous reports,[23,32] which can be calculated as $D^* = R_\lambda/(2eI_{dark}/S)^{1/2}$ and $G = (hc/e\lambda)R_\lambda$, where e is the electron charge, h is the Planck's constant, c is the velocity of light, and λ is the excitation wavelength. Comparing the performance of two kinds of photodetectors at a bias voltage of 1 V with 300 nm UV illumination (0.67 μW/cm^2), without and with decoration of ZnO QDs, the light-to-dark current ratios were 7.9×10^3 and 6.8×10^4, the specific detectivities were 1.1×10^{17} Jones

DOI: 10.1021/acsnano.7b00749
ACS Nano 2017, 11, 4067–4076

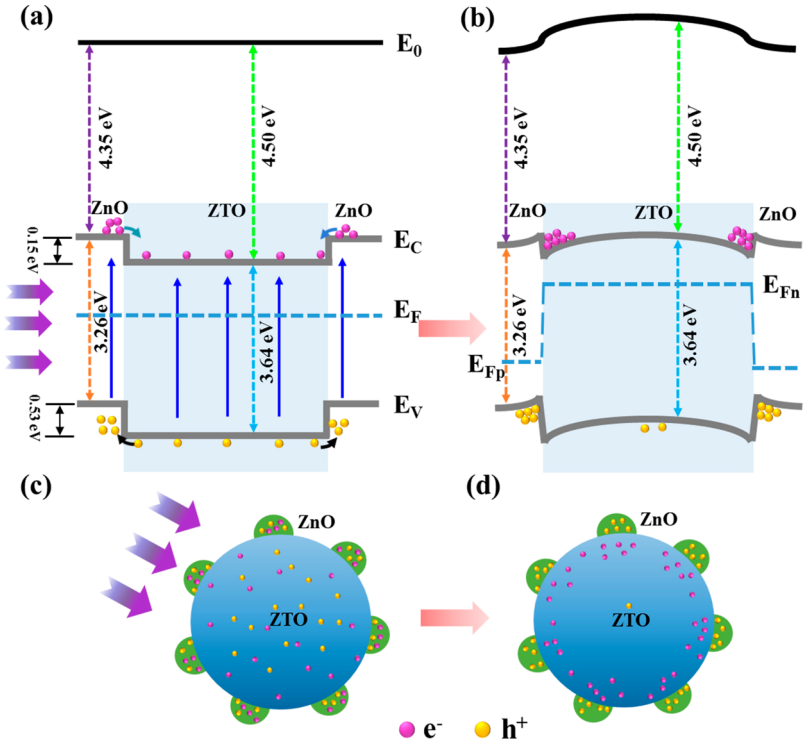

Figure 3. Schematics of performance enhancement mechanism. (a, b) Energy band diagrams and (c, d) corresponding schematics of carrier separation mechanism in the ZnO QD decorated ZTO NW photodetector upon UV illumination.

and 9.0×10^{17} Jones, and the photoconductive gains were 1.3×10^6 and 1.1×10^7, respectively. It can be clearly seen that the performances of the ZTO NW photodetector were dramatically improved by decorating ZnO QDs, and the performance enhancement mechanism will be explained in the latter paragraphs. Interestingly, we have performed device modeling with Silvaco Atlas (Methods section), and the modeled $I-V$ curves are shown in Figure 2c, which is highly consistent with the experimentally measured $I-V$ curves, confirming the performance improvement of the QD-decorated device. Due to the limitation of the simulation tool and too long simulation time for the long nanowire, the length of the simulated nanowire was set as 1 μm, and the voltage range in Figure 2c was proportionally reduced to −0.1 to 0.1 V correspondingly; thus the electric field intensity is maintained.

The reproducibility of photoresponse and response speed are also critical parameters of photodetectors. It remains a huge challenge to achieve a photodetector with both high responsivity and fast response. Figure 2d shows the dynamic photocurrent response curves of two kinds of photodetectors, which are measured by repeatedly turning on and off a 300 nm light with an intensity of 0.67 μW/cm^2 at a bias voltage of 1 V. It can be observed that the light current of the QD-decorated device is 8 times that for the device without QDs. There is no obvious change of the photocurrents for the given seven cycles, revealing the excellent reproducibility and stability of the two devices. Furthermore, the photocurrents of the two devices increase rapidly and reach a steady state when the light is turned on and then decrease quickly after the light is turned off, indicating that the ZnO QD decorated ZTO NW photodetector still possesses a high response speed (over the detection limit of 4200-SCS) like the pristine ZTO NW photodetector. In order to further accurately measure the response time of the photodetector with ZnO QDs, an optical chopper, a current to voltage amplifier (SRS-570), and a digital oscilloscope (Tektroni TDS 2012C) were integrated together as the testing system, as reported in our previous work.[14] The transient response of the photodetector with ZnO QDs is shown in Figure S3a. The response signal clearly increases, reaches a steady state, and then decreases with the change of 300 nm pulsed light illumination at a frequency of 5 Hz. The rise and decay times, which were defined as the time required for the current transition from 10% to 90% (or 90% to 10%) of the steady-state photocurrent, were measured as about 47 and 58 ms (Figure S3b), respectively, which are much faster than those of many other metal oxide NW photodetectors.[15−22] Figure S3c describes the dependence of photocurrent on light intensity of the photodetector with ZnO QDs at a bias voltage of 1 V. The relationship can be expressed as a power law, $I = AP^{\theta}$, where I is the light current, A is a constant, P is the light intensity, and θ is an empirical value.[25] As it can be seen, the experimental values were fitted and give an exponential relationship of $I \sim P^{0.99}$, indicating a near-linear dependence of photocurrent on light intensity.

The experimental results apparently showed that ZnO QD decoration on the ZTO NW surface can drastically improve NW photodetector performance. The mechanism has been investigated, and it can be explained as the following. Compared with ZTO (E_g = 3.64 eV, χ = 4.50 eV), ZnO has a smaller band gap (3.26 eV) and lower electron affinity (4.35 eV). After contacting with ZTO, a type II heterojunction band structure can be formed. Due to the built-in electric field induced by this type II heterojunction, the photogenerated holes migrate to ZnO and are then trapped in QDs near the ZnO/ZTO interface, while the photogenerated electrons stay in ZTO, as shown in Figure 3. These trapped holes in ZnO increase the QD electrostatic potential, thus inducing a positive local gating effect in the n-type NW channel. This positive

DOI: 10.1021/acsnano.7b00749
ACS Nano 2017, 11, 4067−4076

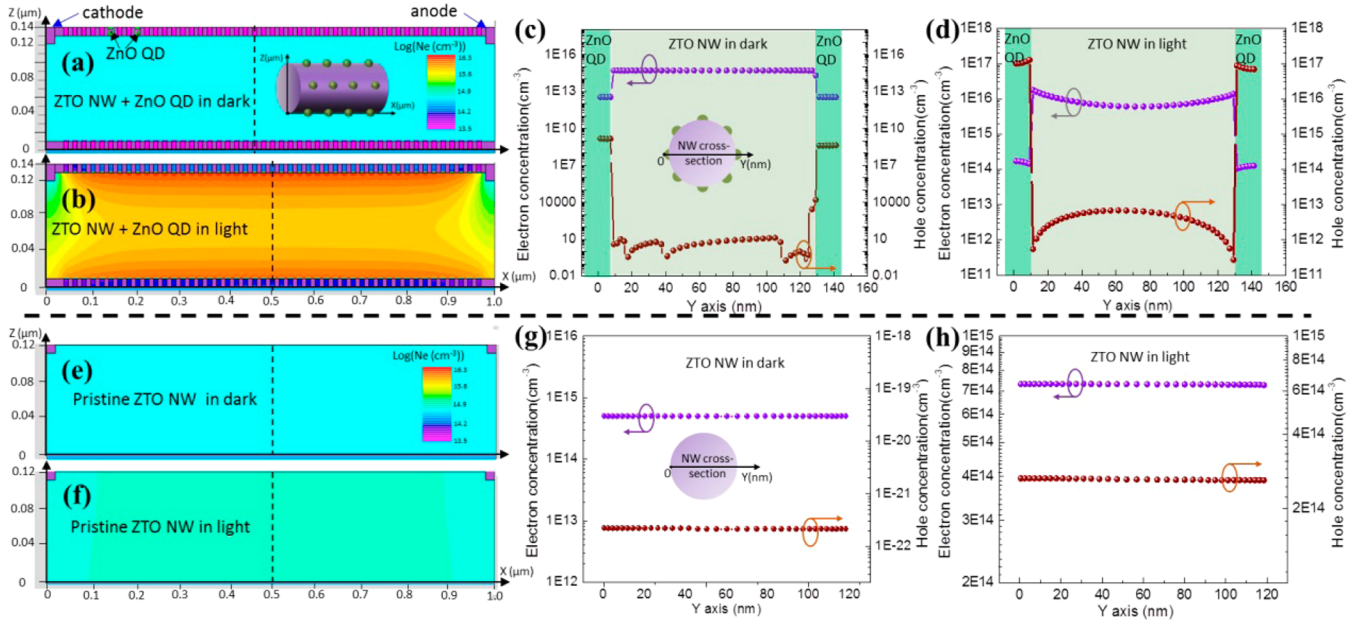

Figure 4. Device modeling of the photodetectors. (a, b) Simulated distributions of electron concentration in the ZnO QD decorated ZTO NW device under dark and 300 nm UV illumination, respectively. The inset in (a) is the model schematic illustration of the ZnO QD decorated ZTO NW. (c, d) Simulated distributions of electron concentration and hole concentration in the cross sections corresponding to the black dotted lines in (a) and (b), respectively. (e, f) Simulated distributions of electron concentration in the pristine ZTO NW device under dark and 300 nm UV illumination, respectively. (g, h) The simulated distributions of electron concentration and hole concentration in the cross sections corresponding to the black dotted lines in (e) and (f), respectively.

surface local gating effect further enhances NW electron concentration in the region close to the interface. Figure S4 exhibits the simulated energy band diagrams of the pristine ZTO NW device and the ZnO QD decorated ZTO NW device under dark and 300 nm UV illumination, respectively. The charge migration process can be further confirmed by the band bending observed in the ZnO QD decorated ZTO NW device under light conditions, as shown in Figure S4d. This overall process leads to three consequences: (1) overall electron concentration in the NW is largely augmented, which increases light current; (2) electrons and holes are effectively separated in the radial direction, thus suppressing recombination and prolonging carrier lifetime; this eventually increases device photoconductive gain; (3) due to surface local positive gating effect, NW surface potential is slightly higher than the core, leading to a marginal upward band bending as shown in Figure 3b.

In order to further verify the rational discussion above, more device simulations were carried out using Silvaco Atlas. Figure 4a,e display the simulated distributions of the electron concentration in the two devices in the dark, respectively, which show that the two devices have almost identical electron concentrations and the distributions of electron concentration in the two devices are uniform, which can also be seen from Figure 4c,g, respectively. These results suggest that under dark conditions, decorating ZnO QDs on a ZTO nanowire does not change the electron concentration and electron distribution in the ZTO nanowire. This is simply due to the fact that ZnO QDs are well isolated; thus, they do not contribute to additional current. However, when comparing Figure 4b and Figure 4f, it can be clearly observed that, under 300 nm UV illumination, the electron concentration in the ZnO QD decorated ZTO NW is much higher than that in the pristine ZTO NW. Moreover, the electron distribution in the pristine ZTO NW is uniform, but the electron distribution in the ZnO QD decorated ZTO NW is rather nonuniform. More details can be seen in Figure 4d, compared with Figure 4h; the ZnO QD decorated ZTO NW has a much higher electron concentration, but lower hole concentration. At the same time, the hole concentration is much higher than the electron concentration in ZnO QDs. This confirms that, under illumination, the type II heterojunction between ZnO and ZTO can drive the migration of photogenerated holes from ZTO NW to ZnO QDs, leaving electrons behind. In addition, as shown in Figure 4d, the electron and hole distribution in ZnO QD decorated ZTO NW are not uniform. The electron concentration in ZTO NW near the ZnO/ZTO interface is higher than that in the center of the ZTO NW, while the hole concentration distribution is opposite, which confirms that the trapped holes in ZnO can induce a local positive gating effect, as discussed above. Note that the marginal increase of hole concentration in the core of the NW, as shown in Figure 4d, cannot significantly increase electron−hole recombination, since the electron concentration is over 3 orders of magnitude higher. Overall, these simulation results further reveal the mechanism accounting for much higher responsivity and photoconductive gain of the ZnO QD decorated ZTO NWs, as compared with the pristine ZTO NWs.

The above investigations are more focused on the response characteristics of the ZnO QD decorated ZTO NW photodetector at room temperature. In fact, thermal stability is also very important for the practical applications of photodetectors. It determines the operating temperature range of devices. In order to assess the photodetection performance of the ZnO QD decorated ZTO NW photodetector in high-temperature environments, the $I-T$ curves of a device as a function of temperatures in the range of 25−125 °C were measured, as shown in Figure S5a, which were performed at a bias voltage of

DOI: 10.1021/acsnano.7b00749
ACS Nano 2017, 11, 4067−4076

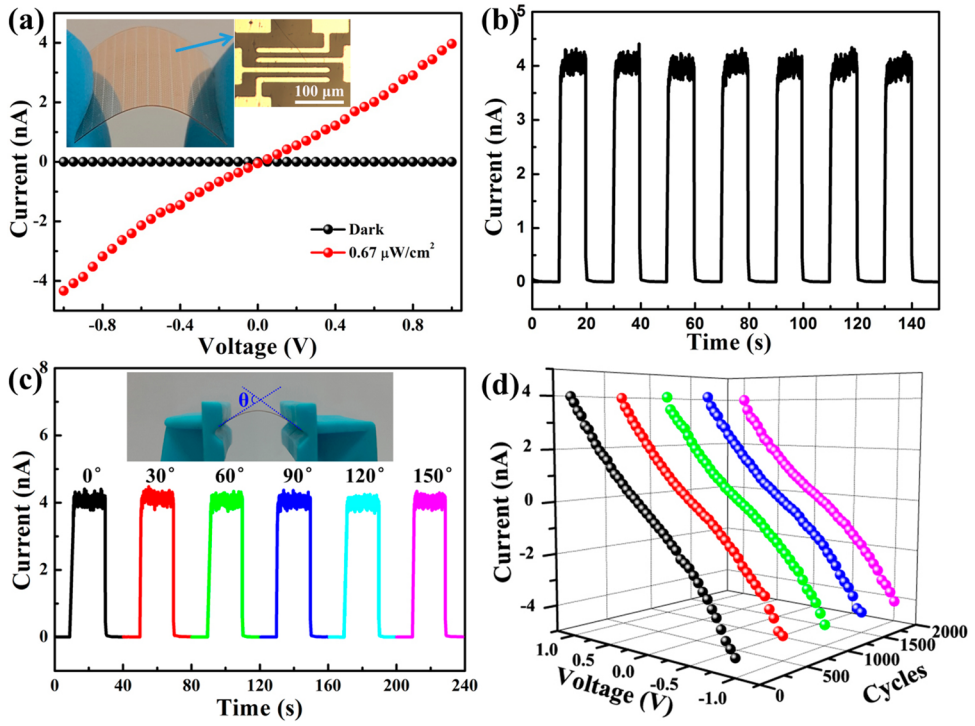

Figure 5. Flexible device performance characterization. (a) *I*−*V* curves of the flexible photodetector under dark and 300 nm UV illumination with a light intensity of 0.67 μW/cm^2. The insets are the optical images of as-fabricated flexible photodetectors on a PET substrate. (b) Photoresponse characteristics of the flexible photodetector at a bias voltage of 1 V with a light intensity of 0.67 μW/cm^2. (c) *I*−*T* curves of the flexible photodetector bent with different bending angles at a bias voltage of 1 V. The inset is the schematic of the bending angle. (d) *I*−*V* curves of the flexible device under 300 nm light illumination after 0, 500, 1000, 1500, and 2000 cycles of bending.

1 V under illumination by 300 nm UV light with a light intensity of 0.67 μW/cm^2. During each measured temperature from 25 to 125 °C, the current of the device sharply increases to a steady state when the light is turned on and then rapidly returns to the dark state after the light is turned off, which shows the high response speed and outstanding reproducibility and stability of the photodetector at each temperature. Moreover, the photodetector can work even at a temperature as high as 125 °C, revealing the wide operating temperature range of the device. In addition, it is noted that the photocurrent decreases with the rise of temperature from 25 to 100 °C and then retains the same value between 100 and 125 °C, but the dark current at 125 °C is slightly higher than that at other temperatures. These phenomena can be explained as follows. As we all know, the conductivity of a semiconductor can be mainly affected by carrier concentration, impurity scattering, and lattice scattering. The impurity scattering usually does not vary with the change of temperature, but intrinsic carrier concentration and lattice scattering increase with rising temperature. Interestingly, the enhancement of carrier concentration will increase the conductivity, whereas the enhancement of lattice scattering will decrease the conductivity, so the result is determined by the dominant mechanism. For the photocurrent, from 25 to 100 °C, the enhancement of intrinsic carrier concentration is not obvious compared with photocarrier concentration, so the effect of lattice scattering is dominant. Therefore, the photocurrent decreases with the rise of temperature from 25 to 100 °C. However, for temperatures from 100 to 125 °C, the effect of the enhancement of intrinsic carrier concentration becomes comparable with the effect of the enhancement of lattice scattering; thus the photocurrent maintains the same value between 100 and 125 °C. In fact, without photocarriers, the effect of the enhancement of intrinsic carrier concentration is more significant in the dark current, which is dominant at the temperature of 125 °C; thus the dark current at 125 °C is higher than that at other temperatures. Furthermore, when the temperature was decreased from 125 to 25 °C, the photocurrent and the dark current recovered to their initial values, revealing the excellent repeatability of the ZnO QD decorated ZTO NW photodetector after high-temperature operation.

Besides thermal stability, long-term stability is also very important for the practical application of photodetectors, which is still a challenging issue for many nanostructured devices since nanomaterials are usually not as stable as bulk materials.[6,28,33] In this regard, we have also examined the long-term stability of the ZnO QD decorated ZTO NW photodetector in ambient air at a bias voltage of 1 V under 300 nm UV illumination. It is worth noting that the device was measured and stored in ambient air at room temperature with 25−40% relative humidity without any encapsulation. As shown in Figure S5b, the spectral responsivity of the device was recorded for 20 weeks. The value of the spectral responsivity shows only marginal fluctuations, which may be caused by the measurement errors. As it can be seen, even after 20 weeks, the spectral responsivity of the device can still retain 99% of the initial value, indicating the excellent long-term stability of the ZnO QD decorated ZTO NW photodetector.

In the past decade, research on flexible electronics has advanced at a fast pace due to the urgent demand for devices with portable, lightweight, and foldable characteristics,[6−9,23−25] and NWs have been considered as promising building blocks for flexible electronics due to their excellent mechanical flexibility.[23−25,34,35] To explore the potential application of

DOI: 10.1021/acsnano.7b00749
ACS Nano 2017, 11, 4067−4076

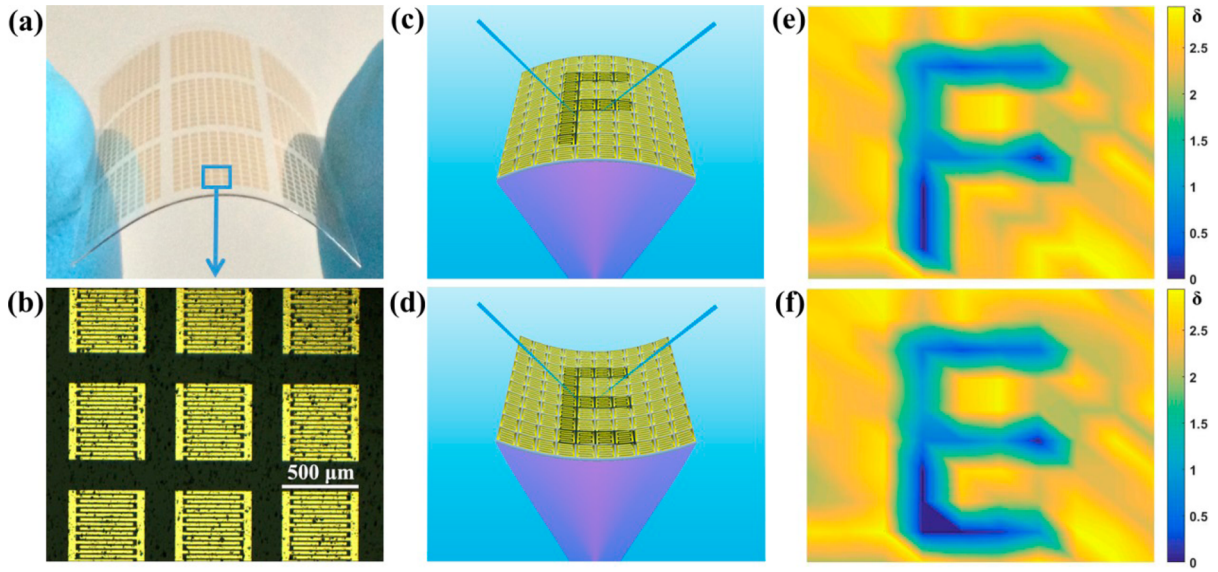

Figure 6. Application of a flexible photodetector array as UV image sensor. (a, b) Optical images of as-fabricated flexible photodetector arrays on a PET substrate. (c, d) Schematic illustrations of using a 10 × 10 flexible photodetector array to sense the letters "F" and "E" under different bending directions, (c) tensile and (d) compressive. The bending angles are both 60°. (e, f) Corresponding output images of letters "F" and "E" by the flexible photodetector array.

the ZnO QD decorated ZTO NWs in flexible photodetectors, devices based on an individual ZnO QD decorated ZTO NW were fabricated on the flexible polyethylene terephthalate (PET) substrate with the aforementioned fabrication process. The inset in the upper left corner of Figure 5a is the optical image of the device, which displays the superior flexibility of the device. Another inset in Figure 5a shows the enlarged view of one photodetector on the flexible PET substrate. The $I-V$ curves of the flexible photodetector under dark and 300 nm UV illumination with a light intensity of 0.67 μW/cm^2 are both displayed in Figure 5a. When the flexible photodetector was irradiated by 300 nm UV light, the current increased dramatically, which illustrates that the flexible photodetector also possesses high sensitivity. Due to the relatively poor contact between the materials and the flexible substrate and low UV reflectance of the PET substrate, the photodetectors based on a flexible substrate usually have a lower photocurrent compared to the photodetectors based on a SiO_2/Si substrate.[35] Figure 5b depicts the dynamic photocurrent response of the flexible photodetector at a bias voltage of 1 V with a light intensity of 0.67 μW/cm^2. It can be seen that the reproducibility and response speed of the flexible photodetector are excellent.

The electrical stability under different bending conditions is a key parameter to evaluate the reliability of flexible electronic devices. Figure 5c exhibits the $I-T$ curves of the flexible photodetector bent with different bending angles at a bias voltage of 1 V. Here the bending angle was defined as the side angle between the two tangents of two ends of the flexible device, as the angle θ shown in the inset of Figure 5c. Different bending angles can be achieved by controlling the two mechanical stages at different distances. It can be seen that both the photocurrent and the dark current of the flexible photodetector nearly stay the same at six different bending angles from 0° to 150°, which demonstrates the excellent electrical stability and mechanical flexibility of the flexible device. Meanwhile, bending/folding cyclability is also important for the practical application of the flexible electric devices. Here a flexible device bent from 0° to 150° and then recovered to 0° was defined as one cycle. Figure 5d displays the $I-V$ curves of the flexible device under 300 nm light illumination before and after different bending cycles. It is clear to see that the $I-V$ curves of the as-fabricated device are almost identical to the $I-V$ curve without bending even after 2000 bending cycles. This result suggests the superior folding endurance of the ZnO QD decorated ZTO NW flexible photodetector.

As an important optoelectronic device, UV image sensors are widely applied in crime investigation, oil spill detecting, fire monitoring, and electrical power line inspection.[1−5] With the fast development of flexible optoelectronics, flexible image sensors have also triggered more and more interest.[6−9] Due to the superior sensitivity, flexibility, and stability, the ZnO QD decorated ZTO NW flexible photodetectors have great potential for flexible UV image sensor applications. To demonstrate this application, flexible photodetectors were integrated into a 10 × 10 array, which works as a 10 × 10 pixel flexible image sensor to sense the letters "F" and "E" under a bending state. Figure 6a shows the optical image of as-fabricated flexible photodetector arrays on a PET substrate under a bending state, which includes nine 10 × 10 arrays, indicating that the pixel number can be increased easily. Figure 6b displays the microscope image of a flexible photodetector array, which is the enlarged view of the blue rectangle area in Figure 6a. It can be seen that every flexible photodetector is composed of two interdigital electrodes; the gap between two electrodes is about 10 μm. The structure allows the NWs to connect to two electrodes easily, which ensures that all flexible photodetectors are functional. The area of a flexible photodetector is about 0.5 × 0.5 mm^2, which can be further reduced considering the small size of the NWs. Figure 6c,d depict the schematic illustrations of using a 10 × 10 flexible photodetector array to image the letters "F" and "E" under different bending directions. To facilitate the measurement, the patterns of the letters "F" and "E" were placed on the back of the device and the device was irradiated from the back by the incident light. Due to the strong absorption of PET to 300 nm light, as shown

DOI: 10.1021/acsnano.7b00749
ACS Nano 2017, 11, 4067−4076

in Figure S6, 350 nm light with an intensity of 10 μW/cm^2 was used as the incident light. Two probes on the top of the device can collect the testing data easily. In order to show the letters "F" and "E", the denary logarithm of the photodark current ratio, denoted by the letter δ ($\delta = \log_{10}(I_{light}/I_{dark})$), of each flexible photodetector was recorded. The flexible photodetectors in the array that were blocked by the letter pattern displayed very low values, while the remaining flexible photodetectors displayed higher values. It can be observed that, under different bending directions, the images of the letters "F" and "E" can both be displayed clearly, as shown in Figure 6e,f. This result indicates that the flexible photodetector array is reliable for UV photosensitive imaging.

CONCLUSIONS

In summary, high-quality ZnO QD decorated ZTO NWs were synthesized *via* a facile two-step method. Systematic investigations on the photoresponse characteristics of individual ZnO QD decorated ZTO NW photodetectors based on a rigid SiO_2/Si substrate have been carried out, which reveal their superior device performance, such as ultrahigh light-to-dark current ratio (up to 6.8×10^4), specific detectivity (up to 9.0×10^{17} Jones) and photoconductive gain (up to 1.1×10^7), high response speed (47 ms), and excellent thermal stability and long-term stability (>20 weeks in air). Further analysis by simulation shows that their excellent photodetection properties originate from the rational band engineering at the QD/NW interface, which results in effective separation of electron−hole pairs. Consequently it can increase the electron concentration and reduce the recombination of carriers in ZTO NWs. At the same time, hole trapping in ZnO QDs induces a local positive gating effect to NWs, which further enhances electron concentration in the NWs. Overall this mechanism can improve responsivity of a NW photodetector by 1 order of magnitude after ZnO QD decoration. The intriguing enhancement mechanism discovered in this work can also be used to guide the design of high-performance photodetectors based on other nanomaterials. In addition, flexible photodetectors based on a flexible PET substrate were also fabricated and displayed outstanding flexibility, electrical stability, and folding endurance. Furthermore, the flexible photodetectors were integrated into a 10 × 10 array, which demonstrated the application as a high-performance flexible image sensor. The results indicate that the as-synthesized ZnO QD decorated ZTO NWs have a highly promising application potential in future flexible optoelectronics beyond UV imaging.

METHODS

Synthesis of ZTO NWs. A mixture of 20 mg of Zn and 9 mg of Sn powder was placed in an alumina boat at the center of a tube furnace as the source material. A silicon wafer coated with a ∼10 nm thick Au layer as the catalyst was then placed face-down above the source material to ensure high vapor pressure and to collect the growth products. Once the growth process started, the temperature of the furnace was rapidly raised to 1000 °C in 30 min and kept at that temperature for 30 min. The flow rate of N_2 was kept at 80 sccm (standard cubic centimeters per minute). Finally, as the reaction was completed, the furnace was cooled to room temperature naturally, and a white product was found deposited on the substrate.

Decorating ZnO QDs on ZTO NWs. The as-prepared ZTO NWs were put in a Teflon-lined stainless steel autoclave (50 mL volume), and 25 mL of zinc acetate dihydrate in absolute ethanol (0.02 M) was added. The sealed autoclave was then heated to 95 °C and maintained for 2 h for solvothermal growth of ZnO QDs on the ZTO NW surface.

Device Fabrication and Measurements. To fabricate single-nanowire photodetectors, pristine ZTO NWs or ZTO NWs with ZnO QDs were first dispersed into 2-propanol solvent from the Si substrate by a sonication process. The mixture was then dropped onto two different kinds of substrates, namely, a rigid SiO_2/Si substrate and a flexible PET substrate. Subsequently, a conventional photolithography was used to pattern the source and drain electrodes, followed by a thermal evaporation and lift-off process to achieve Cr/Au electrodes with a thickness of 10 nm/50 nm. The fabrication process of the NW photodetector array is similar to the above process, except that the concentration of NW solution was increased to ∼4 mg/mL. The photoresponse of the devices was measured by a probe station with a Keithley 4200-SCS semiconductor parameter analyzer. A power-adjustable xenon lamp (CEL-HXUV300) was used as the illumination source for photoresponse measurements. An optical chopper, a current to voltage amplifier (SRS-570), and a digital oscilloscope (Tektronix TDS 2012C) were integrated together to measure the response speed of the photodetectors. The incident power of the light was measured using an Ophir NOVA power meter. All measurements were performed in air.

Material Characterizations. The sizes and morphologies of the as-synthesized products were characterized by a scanning electron microscope (Zeiss Supra55 (VP)) and a transmission electron microscope (JEM-2010F) equipped with an energy-dispersive X-ray analyzer. The crystallinity of the products was analyzed *via* a powder X-ray diffractometer (Rigaku D/Max-2550, λ = 1.5418 Å).

Device Physics Simulation. The device physics simulations were performed with Silvaco Atlas (version 5.19.20.R) on a ZnO QD decorated ZTO NW and a pristine ZTO NW. Figure 4 shows the simulation results using a 3-D cylindrical model. The simulated ZTO NW has a diameter of 120 nm and length of 1 μm. To facilitate the simulation, the hemispherical ZnO QDs were simplified into a square shape with side of 10 nm and center-to-center distance of 20 nm. These QDs were uniformly distributed on the top and bottom of a ZTO NW. The specific material parameters used are displayed in Table S1. An anode and cathode were put on two ends of the NW, and the contacts were regarded as ohmic contacts. In the simulations, the finite-difference time-domain method was utilized to achieve optical generation inside the NWs. A simulated 300 nm wavelength UV light with an intensity of 0.67 μW/cm^2 was used as light source. The resulting $I-V$ curves of two kinds of photodetectors are plotted in Figure 2d. The energy band diagrams of the two devices under dark and light are plotted in Figure S4. The distributions of electron concentration and hole concentration in the two devices under dark and light are plotted in Figure 4.

ASSOCIATED CONTENT

Supporting Information

The Supporting Information is available free of charge on the ACS Publications website at DOI: 10.1021/acsnano.7b00749.

EDX spectrum and XRD pattern of the as-synthesized ZTO NWs; TEM and HRTEM images of the as-synthesized ZTO NW with ZnO QDs; STEM image and corresponding elemental mapping showing the dispersion of O, Zn, and Sn in the ZTO NW with ZnO QDs; transient response of photodetector made of the ZnO QD decorated ZTO NW chopped at a frequency of 5 Hz under 300 nm light illumination; enlarged view of one cycle of the transient response of photodetector; dependence of photocurrent on light intensity; simulated energy band diagrams of the devices under dark and light; thermal and long-term stability of the photodetectors; specific material parameters used in device simulation; transmittance spectrum of the PET substrate (PDF)

DOI: 10.1021/acsnano.7b00749
ACS Nano 2017, 11, 4067−4076

AUTHOR INFORMATION

Corresponding Authors

*E-mail: eezfan@ust.hk.

*E-mail: gzshen@semi.ac.cn.

ORCID

Zhiyong Fan: 0000-0002-5397-0129

Author Contributions

L.L., L.G., Z.L., Z.F., and G.S. designed the experiments. L.L., Z.L., and G.S. carried out the experiments. L.G. and Z.F. performed Silvaco simulations. L.L., L.G., Z.L., Z.F., and G.S. contributed to data analysis. L.L. and Z.F. wrote the paper, and all authors provided feedback.

Author Contributions

§L. Li and L. Gu contribute equally to this work.

Notes

The authors declare no competing financial interest.

ACKNOWLEDGMENTS

This work was supported by the National Natural Science Foundation of China (61377033, 61625404, 61574132, 61504136), General Research Fund (project 16237816) from the Hong Kong Research Grant Council, the Hong Kong Innovation and Technology Fund (ITS/362/14FP) from the Innovation and Technology Commission, Beijing Natural Science Foundation (4162062), Key Research Program of Frontiers Sciences, CAS (QYZDY-SSW-JSC004), The Center for 1D/2D Quantum Materials, and State Key Laboratory on Advanced Displays and Optoelectronics at HKUST.

REFERENCES

(1) Leintz, R.; Bond, J. W. Can the RUVIS Reflected UV Imaging System Visualize Fingerprint Corrosion on Brass Cartridge Casings Postfiring? *J. Forensic Sci.* **2013**, *58*, 772−775.

(2) Fingas, M.; Brown, C. Review of Oil Spill Remote Sensing. *Mar. Pollut. Bull.* **2014**, *83*, 9−23.

(3) Cheong, P.; Chang, K. F.; Lai, Y. H.; Ho, S. K.; Sou, I. K.; Tam, K. W. A ZigBee-Based Wireless Sensor Network Node for Ultraviolet Detection of Flame. *IEEE T. Ind. Electron.* **2011**, *58*, 5271−5277.

(4) Zhou, W.; Li, H.; Yi, X.; Tu, J.; Yu, J. A Criterion for UV Detection of AC Corona Inception in a Rod-Plane Air Gap. *IEEE Trans. Dielectr. Electr. Insul.* **2011**, *18*, 232−237.

(5) Li, Z.; Li, L.; Jiang, X.; Hu, J.; Zhang, Z.; Zhang, W. Effects of Different Factors on Electrical Equipment UV Corona Discharge Detection. *Energies* **2016**, *9*, 369.

(6) Gu, L.; Tavakoli, M. M.; Zhang, D.; Zhang, Q.; Aashir, W.; Xiao, Y.; Tsui, K.; Lin, Y.; Liao, L.; Wang, J.; et al. 3D Arrays of 1024-Pixel Image Sensors Based on Lead Halide Perovskite Nanowires. *Adv. Mater.* **2016**, *28*, 9713−9721.

(7) Kim, J.; Kim, J.; Jo, S.; Kang, J.; Jo, J. W.; Lee, M.; Moon, J.; Yang, L.; Kim, M. G.; Kim, Y. H. Ultrahigh Detective Heterogeneous Photosensor Arrays with In-Pixel Signal Boosting Capability for Large-Area and Skin-Compatible Electronics. *Adv. Mater.* **2016**, *28*, 3078−3086.

(8) Chu, Y.; Wu, X.; Lu, J.; Liu, D.; Du, J.; Zhang, G.; Huang, J. Photosensitive and Flexible Organic Field-Effect Transistors Based on Interface Trapping Effect and Their Application in 2D Imaging Array. *Adv. Sci.* **2016**, *8*, 1500435.

(9) Deng, H.; Yang, X.; Dong, D.; Li, B.; Yang, D.; Yuan, S.; Qiao, K.; Cheng, Y. B.; Tang, J.; Song, H. Flexible and Semitransparent Organolead Triiodide Perovskite Network Photodetector Arrays with High Stability. *Nano Lett.* **2015**, *15*, 7963−7969.

(10) Zhao, B.; Wang, F.; Chen, H.; Wang, Y.; Jiang, M.; Fang, X.; Zhao, D. Solar-Blind Avalanche Photodetector Based On Single ZnO-Ga_2O_3 Core-Shell Microwire. *Nano Lett.* **2015**, *15*, 3988−3993.

(11) Wang, X.; Zhang, Y.; Chen, X.; He, M.; Liu, C.; Yin, Y.; Zou, X.; Li, S. Ultrafast, Superhigh Gain Visible-Blind UV Detector and Optical Logic Gates Based on Nonpolar A-axial GaN Nanowire. *Nanoscale* **2014**, *6*, 12009−12017.

(12) Wang, X.; Yu, R.; Peng, W.; Wu, W.; Li, S.; Wang, Z. L. Temperature Dependence of the Piezotronic and Piezophototronic Effects in A-axis GaN Nanobelts. *Adv. Mater.* **2015**, *27*, 8067−8074.

(13) Chen, R. S.; Yang, T. H.; Chen, H. Y.; Chen, L. C.; Chen, K. H.; Yang, Y. J.; Su, C. H.; Lin, C. R. High-Gain Photoconductivity in Semiconducting InN Nanowires. *Appl. Phys. Lett.* **2009**, *95*, 162112.

(14) Lou, Z.; Li, L.; Shen, G. Ultraviolet/visible Photodetectors with Ultrafast, High Photosensitivity Based on 1D ZnS/CdS Heterostructures. *Nanoscale* **2016**, *8*, 5219−5225.

(15) Kind, H.; Yan, H.; Messer, B.; Law, M.; Yang, P. Nanowire Ultraviolet Photodetectors and Optical Switches. *Adv. Mater.* **2002**, *14*, 158−160.

(16) Fan, Z.; Chang, P. C.; Lu, J. G.; Walter, E. C.; Penner, R. M.; Lin, C. H.; Lee, H. P. Photoluminescence and Polarized Photodetection of Single ZnO Nanowires. *Appl. Phys. Lett.* **2004**, *85*, 6128−6130.

(17) Li, Y.; Tokizono, T.; Liao, M.; Zhong, M.; Koide, Y.; Yamada, I.; Delaunay, J. J. Efficient Assembly of Bridged β-Ga_2O_3 Nanowires for Solar-Blind Photodetection. *Adv. Funct. Mater.* **2010**, *20*, 3972−3978.

(18) Zhang, D.; Li, C.; Han, S.; Liu, X.; Tang, T.; Jin, W.; Zhou, C. Ultraviolet Photodetection Properties of Indium Oxide Nanowires. *Appl. Phys. A: Mater. Sci. Process.* **2003**, *77*, 163−166.

(19) Fu, X. Q.; Wang, C.; Feng, P.; Wang, T. H. Anomalous Photoconductivity of CeO_2 Nanowire in Air. *Appl. Phys. Lett.* **2007**, *91*, 073104.

(20) Hu, L. F.; Yan, J.; Liao, M. Y.; Wu, L. M.; Fang, X. S. Ultrahigh External Quantum Efficiency from Thin SnO_2 Nanowire Ultraviolet Photodetectors. *Small* **2011**, *7*, 1012−1017.

(21) Zhai, T.; Fang, X.; Liao, M.; Xu, X.; Zeng, H.; Yoshio, B.; Golberg, D. A Comprehensive Review of One-Dimensional Metal-Oxide Nanostructure Photodetectors. *Sensors* **2009**, *9*, 6504−6529.

(22) Tian, W.; Lu, H.; Li, L. Nanoscale Ultraviolet Photodetectors Based on One Dimensional Metal Oxide Nanostructures. *Nano Res.* **2015**, *8*, 382−405.

(23) Liu, X.; Gu, L.; Zhang, Q.; Wu, J.; Long, Y.; Fan, Z. All-Printable Band-Edge Modulated ZnO Nanowire Photodetectors with Ultra-High Detectivity. *Nat. Commun.* **2014**, *5*, 4007.

(24) Liu, Z.; Xu, J.; Chen, D.; Shen, G. Flexible Electronics Based on Inorganic Nanowires. *Chem. Soc. Rev.* **2015**, *44*, 161−192.

(25) Lou, Z.; Li, L.; Shen, G. High-Performance Rigid and Flexible Ultraviolet Photodetectors with Single-Crystalline $ZnGa_2O_4$ Nanowires. *Nano Res.* **2015**, *8*, 2162−2169.

(26) Cheng, B.; Xu, J.; Ouyang, Z.; Su, X.; Xiao, Y.; Lei, S. Individual Ohmic Contacted ZnO/Zn_2SnO_4 Radial Heterostructured Nanowires as Photodetectors with a Broad-Spectral-Response: Injection of Electrons into/from Interface States. *J. Mater. Chem. C* **2014**, *2*, 1808−1814.

(27) Chen, J.; Lu, L.; Wang, W. Zn_2SnO_4 Nanowires as Photoanode for Dye-Sensitized Solar Cells and the Improvement on Open-Circuit Voltage. *J. Phys. Chem. C* **2012**, *116*, 10841−10847.

(28) Zhang, Y.; Wang, J.; Zhu, H.; Li, H.; Jiang, L.; Shu, C.; Hu, W.; Wang, C. High Performance Ultraviolet Photodetectors Based on an Individual Zn_2SnO_4 Single Crystalline Nanowire. *J. Mater. Chem.* **2010**, *20*, 9858−9860.

(29) Lou, Z.; Li, L.; Shen, G. $InGaO_3(ZnO)$ Superlattice Nanowires for High-Performance Ultraviolet Photodetectors. *Adv. Electron. Mater.* **2015**, *1*, 1500054.

(30) Lim, T.; Kim, H.; Meyyappan, M.; Ju, S. Photostable Zn_2SnO_4 Nanowire Transistors for Transparent Displays. *ACS Nano* **2012**, *6*, 4912−4920.

(31) Wu, F.; Zhao, Y.; Zhang, H.; Tong, Y. H. Device Architecture Engineering in Polymer/ZnO Quantum dots/ZnO Array Ternary Hybrid Solar Cells. *Appl. Phys. A: Mater. Sci. Process.* **2015**, *120*, 941−947.

DOI: 10.1021/acsnano.7b00749
ACS Nano 2017, 11, 4067−4076

(32) Li, L.; Lou, Z.; Shen, G. Hierarchical CdS Nanowires Based Rigid and Flexible Photodetectors with Ultrahigh Sensitivity. *ACS Appl. Mater. Interfaces* **2015**, *7*, 23507−23514.
(33) Li, X.; Dar, M. I.; Yi, C.; Luo, J.; Tschumi, M.; Zakeeruddin, S. M.; Nazeeruddin, M. K.; Han, H.; Gratzel, M. Improved Performance and Stability of Perovskite Solar Cells by Crystal Crosslinking with Alkylphosphonic Acid ω-Ammonium Chlorides. *Nat. Chem.* **2015**, *7*, 703−711.
(34) Liu, Z.; Huang, H.; Liang, B.; Wang, X.; Wang, Z.; Chen, D.; Shen, G. Zn_2GeO_4 and $In_2Ge_2O_7$ Nanowire Mats Based Ultraviolet Photodetectors on Rigid and Flexible Substrates. *Opt. Express* **2012**, *20*, 2982−2991.
(35) Chen, G.; Liang, B.; Liu, X.; Liu, Z.; Yu, G.; Xie, X.; Luo, T.; Chen, D.; Zhu, M.; Shen, G. High-Performance Hybrid Phenyl-C61-Butyric Acid Methyl Ester/Cd_3P_2 Nanowire Ultraviolet-Visible-Near Infrared Photodetectors. *ACS Nano* **2014**, *8*, 787−796.

DOI: 10.1021/acsnano.7b00749
ACS Nano 2017, 11, 4067−4076